Molecular Biology of the Cell
Vol. 11, 4131–4142, December 2000

Complex Phenotype of Mice Lacking Occludin, a Component of Tight Junction Strands

Mitinori Saitou,* Mikio Furuse,* Hiroyuki Sasaki,† Jörg-Dieter Schulzke,‡ Michael Fromm,§ Hiroshi Takano,‖¶ Tetsuo Noda,‖¶ and Shoichiro Tsukita*#

*Department of Cell Biology, Kyoto University Faculty of Medicine, Sakyo-ku, Kyoto 606-8501, Japan; †KAN Research Institute Inc., Kyoto Research Park, Chudoji, Shimogyo-ku, Kyoto 600-8317, Japan; ‡Medizinische Klinik I Gastroenterologie und Infektiologie and §Institut für Klinische Physiologie, Universitätsklinikum Benjamin Franklin, Freie Universität Berlin, Berlin, Germany; ‖Department of Cell Biology, Cancer Institute, Toshima-ku, Tokyo 170-8455, Japan; and ¶Department of Molecular Genetics, Tohoku University School of Medicine, Sendai 980-8575, Japan

Submitted July 24, 2000; Revised September 14, 2000; Accepted September 28, 2000
Monitoring Editor: W. James Nelson

Occludin is an integral membrane protein with four transmembrane domains that is exclusively localized at tight junction (TJ) strands. Here, we describe the generation and analysis of mice carrying a null mutation in the occludin gene. Occludin −/− mice were born with no gross phenotype in the expected Mendelian ratios, but they showed significant postnatal growth retardation. Occludin −/− males produced no litters with wild-type females, whereas occludin −/− females produced litters normally when mated with wild-type males but did not suckle them. In occludin −/− mice, TJs themselves did not appear to be affected morphologically, and the barrier function of intestinal epithelium was normal as far as examined electrophysiologically. However, histological abnormalities were found in several tissues, i.e., chronic inflammation and hyperplasia of the gastric epithelium, calcification in the brain, testicular atrophy, loss of cytoplasmic granules in striated duct cells of the salivary gland, and thinning of the compact bone. These phenotypes suggested that the functions of TJs as well as occludin are more complex than previously supposed.

INTRODUCTION

Tight junctions (TJs) are one mode of cell-to-cell adhesion, and play a central role in sealing the intercellular space in epithelial and endothelial cellular sheets (reviewed in Gumbiner, 1987, 1993; Schneeberger and Lynch, 1992; Anderson and van Itallie, 1995; Goodenough, 1999). TJs are also thought to be involved in creating and establishing apical and basolateral membrane domains in these types of cells (Rodriguez-Boulan and Nelson, 1989). Through these "barrier" and "fence" functions of TJs, epithelial/endothelial cellular sheets establish various compositionally distinct fluid compartments. Therefore, TJs are considered to be fundamental structures in multicellular organisms. On ultrathin-section electron microscopy, TJs appear as a series of discrete sites of apparent fusion, involving the outer leaflet of the plasma membrane of adjacent cells (Farquhar and Palade, 1963). On freeze-fracture electron microscopy, TJs appear as a set of continuous, anastomosing intramembranous particle strands (TJ strands or fibrils) in the P-face (the outwardly facing cytoplasmic leaflet) with complementary grooves in the E-face (the inwardly facing extracytoplasmic leaflet) (Staehelin, 1973, 1974). These morphological findings led to the following structural model for TJs: Within the lipid bilayer of each membrane, the TJ strands, which are probably composed of linearly aggregated integral membrane proteins, form networks through their ramification (Tsukita and Furuse, 2000). Each TJ strand laterally and tightly associates with that in the opposing membrane of adjacent cells to form a paired strand, where the intercellular distance becomes almost zero.

Occludin with a molecular mass of ~65 kDa was identified as the first component of the TJ strand itself (Furuse *et al.*, 1993; Ando-Akatsuka *et al.*, 1996; Saitou *et al.*, 1997). Occludin is comprised of four transmembrane domains, a long COOH-terminal cytoplasmic domain, a short NH_2-terminal cytoplasmic domain, two extracellular loops, and one intracellular turn. One of the most characteristic aspects of its sequence is the high content of tyrosine and glycine residues in the first extracellular loop (~60%). Occludin has been shown to be a functional component of TJs. Overexpression of full-length occludin in cultured Madin-Darby canine kidney (MDCK) cells elevates their transepithelial

Corresponding author. E-mail address: htsukita@mfour.med.kyoto-u.ac.jp.

resistance (McCarthy *et al.*, 1996), and introduction of COOH-terminally truncated occludin into MDCK cells or *Xenopus* embryo cells results in increased paracellular leakage of small molecular mass tracers (Balda *et al.*, 1996; Chen *et al.*, 1997). The transepithelial resistance of cultured *Xenopus* epithelial cells is down-regulated by addition to the culture medium of a synthetic peptide corresponding to the second extracellular loop of occludin (Wong and Gumbiner, 1997). The TJ fence function is also affected when COOH-terminally truncated occludin is introduced into MDCK cells (Balda *et al.*, 1996). On the other hand, it has become clear that the structure and functions of TJs cannot be explained by occludin alone. For example, although TJ strands in most cells contain occludin, those in endothelial cells of non-neuronal tissues as well as in Sertoli cells in the human testis appear to lack occludin (Hirase *et al.*, 1997; Moroi *et al.*, 1998). More conclusively, when both alleles of the occludin gene were disrupted in embryonic stem (ES) cells, visceral endoderms differentiated from these cells still bore well-developed TJ strands (Saitou *et al.*, 1998). This finding not only indicated that there are as yet unidentified TJ integral membrane protein(s) that can form TJ strands without occludin but also urged us to reconsider the function of occludin in TJ strands.

Recently, two related ~23-kDa integral membrane proteins, claudin-1 and -2 (38% identical at the amino acid sequence level), were identified as the second and third components of TJ strands (Furuse *et al.*, 1998a). Both claudin-1 and -2 also possess four transmembrane domains, but do not show any sequence similarity to occludin. The cytoplasmic domain and the second extracellular loop of claudins are significantly shorter than those of occludin, and their first extracellular loop is not enriched in tyrosine or glycine residues. Claudins comprise a large gene family consisting of more than 20 members (Morita *et al.*, 1999a–c; Tsukita and Furuse, 1999, 2000). Interestingly, when these claudins were singly expressed into fibroblasts lacking TJs, well-developed networks of TJ strands were reconstituted between adjacent transfectants, indicating that claudins, not occludin, constitute the backbone of TJ strands (Furuse *et al.*, 1998b). When occludin was cointroduced into fibroblasts together with claudins, occludin was incorporated into the claudin-based reconstituted TJ strands (Furuse *et al.*, 1998b).

These observations have then naturally raised the question of the physiological function of occludin. As noted above, without occludin TJ strands themselves can be formed at the cellular level (Saitou *et al.*, 1998). In this study, to explore the in vivo function of occludin, we disrupted the endogenous mouse occludin locus. Both heterozygous and homozygous mutant mice were viable, but the homozygous mutant mice showed very complex abnormalities in various organs.

MATERIALS AND METHODS

Antibodies

Rat anti-mouse occludin monoclonal antibody (mAb) (MOC37) was raised against the cytoplasmic domain of mouse occludin produced in *Escherichia coli* (Saitou *et al.*, 1997). Rabbit anti-mouse claudin-3 polyclonal antibody was raised and characterized previously (Morita *et al.*, 1999a).

Targeting Vectors, Gene Targeting, and Generation of Occludin-deficient Mice

A λ phage 129/Sv mouse genomic library was screened by using mouse occludin cDNA (nucleotide 1–424) as a probe, and the overall structure of the mouse occludin genomic locus was determined as described previously (Figure 1) (Saitou *et al.*, 1998).

The targeting vectors were designed to delete the entire sequence of putative exon 3 (nucleotide 273–945). Targeting vector I was constructed by ligating a 7.5-kb *Bam*HI fragment and a 2.4-kb *Apa*I/*Eco*RI fragment, which were located upstream and downstream of exon 3, respectively, to loxP-*pgk* neo-loxP cassette. The transcriptional orientation of *pgk* neo was opposite to that of occludin. The targeting vector II was constructed as described previously (Saitou *et al.*, 1998).

Gene targeting and analyses of singly integrated correct homologous recombinants were conducted as described previously (Saitou *et al.*, 1998). One ES cell clone with targeting vector I and two clones with targeting vector II were injected into C57BL/6 blastocysts for the generation of chimeric mice. Chimeric male mice were mated with C57BL/6 females, and agouti offspring were generated from all of the clones, indicating germ line transmission of the ES cell genome.

The genotype of offspring was analyzed by Southern blotting and polymerase chain reaction (PCR) by using tail DNA as a template. For PCR, to amplify the 476-bp wild-type fragment of the occludin genomic clone, the 255-bp targeted locus with vector I, or the 231-bp targeted locus with vector II, the following primer pairs were designed, respectively: [P1, 5′-ATAAGTCAGCCTGGCATCTCC-3′; P2, 5′-TCAAGTTTCCAGCTGATGCAG-3′], [P1; P3,5′-GTTCCACATACACTTCATTCTCAG-3′], or [P1; P4, 5′-TCTCTAGAGGATCCTAGATGC-3′]. Heterozygous mice were then interbred to produce homozygous mice.

Reverse Transcription (RT)-PCR

Total RNA was isolated from the liver and kidney of wild-type, heterozygous, and homozygous mice by using guanidinium isothiocyanate and acid phenol/chloroform (Chomczynski and Sacchi, 1987). First strand cDNA synthesis and subsequent PCR were conducted as described previously (Saitou *et al.*, 1998). Briefly, primers (upstream, 5′-TTGGGACAGAGGCTATGG-3′; downstream, 5′-ACCCACTCTTCAACATTGGG-3′) were designed to amplify a portion of occludin cDNA (nucleotide 487-1109). As a control for the presence of amplifiable RNA, hypoxanthine phosphoribosyl transferase primers were designed as previously described (Keller *et al.*, 1993).

Immunofluorescence Microscopy

Mouse intestine was dissected and frozen in liquid N_2. Frozen sections ~7 μm in thickness were cut and processed for indirect immunofluorescence microscopy as described previously (Saitou *et al.*, 1997).

Electron Microscopy

Ultrathin-section and freeze-fracture replica electron microscopy were performed as described previously (Saitou *et al.*, 1998). Ultrathin sections and freeze-fracture replicas were observed by using a 1200EX electron microscope (JEOL, Tokyo, Japan) at an acceleration voltage of 100 kV.

Histological Analyses

Mouse tissues were dissected and fixed with 10% formalin in phosphate-buffered saline at 4°C for 3 d. Samples were then dehydrated through a graded series of ethanol, and embedded in polyester or paraffin wax. Sections ~5 μm in thickness were cut on a microtome, stained with hematoxylin-eosin, and examined by using a Zeiss Axiophot II photomicroscope (Carl Zeiss, Inc., Thornwood, NY).

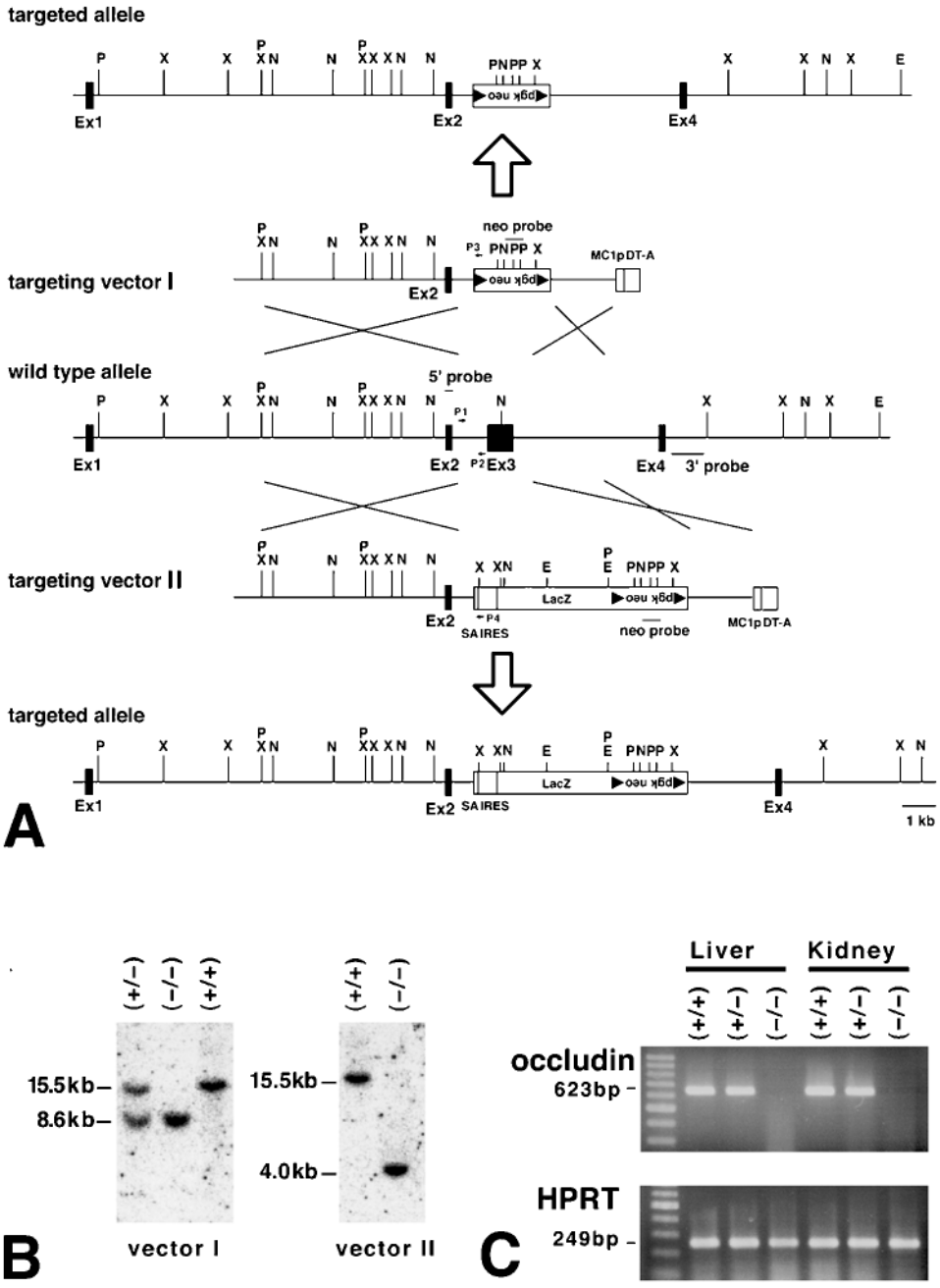

Figure 1. Generation of occludin −/− mice. (A) Restriction maps of the wild-type allele, targeting vectors I and II, and the respective targeted alleles of the mouse occludin gene. The first ATG codon was located in exon 2; exon 3 encoded the NH_2-terminal half of the occludin molecule from the first transmembrane domain to the second extracellular loop. Exon 4 encoded the fourth transmembrane domain and the initial part of the COOH-terminal cytoplasmic domain, indicating the existence of one or more downstream exons. The targeting vectors I and II contained the loxP/*pgk* neo/loxP cassette and SA IRES/LacZ/loxP/*pgk* neo/loxP cassette, respectively, in their middle portion to delete exon 3 in the targeted alleles. The positions of 5′, 3′, and neo probes for Southern blotting are indicated by bars (5′ probe, 3′ probe, and neo probe), and those of primers for PCR are indicated by arrows (P1, P2, P3, P4; see MATERIALS AND METHODS). The loxP sequence is shown by closed triangles. P, *Pst*I; X, *Xba*I; N, *Nco*I; E, *Eco*RV. (B) Genotype analyses by Southern blotting of *Xba*I-digested genomic DNA from animals that were wild-type (+/+) or either heterozygous (+/−) or homozygous (−/−) for the mutant occludin gene allele. Southern blotting with the 5′ probe yielded a 15.5-kb band, an 8.6-kb band, and a 4.0-kb band from the wild-type allele, vector I-, and vector II-targeted alleles, respectively. 3′ and neo probes were used to confirm the correct targeting. Genotyping was also performed by PCR with primers such as P1, P2, P3, and P4 (our unpublished results). (C) Loss of occludin mRNA in the liver and kidney of occludin −/− mice examined by RT-PCR. Occludin expression was abolished in occludin −/− mice, but not in wild-type or occludin +/− mice. As a control, the hypoxanthine phosphoribosyl transferase gene was equally amplified in all samples.

Measurement of Epithelial Resistance

Intact (i.e., not stripped) mouse ileum or distal colon was mounted in Ussing chambers designed for AC impedance analysis (Gitter *et al.*, 1998). This technique allows to determine the epithelial (R^e) and the subepithelial (R^{sub}) portion of the total wall resistance (R^t) of mouse intestine (Gitter *et al.*, 2000). Briefly, the voltage responses after transepithelial application of 35 $\mu A/cm^2$ eff. sine-wave AC of 48 discrete frequencies in a range from 1 to 65 kHz were detected by phase-sensitive amplifiers (model 1250 frequency response analyzer and model 1286 electrochemical interface; Solartron Schlumberger, Farnborough Hampshire, Great Britain). Complex impedance values were calculated and corrected for the resistance of the bathing solution and the frequency behavior of the measuring setup for each frequency. Then, the impedance locus was plotted in a Nyquist diagram and a circle segment was fitted by least-square analysis. From this circle segment, three variables of an electric equivalent circuit were obtained, which consisted of a resistor and a capacitor in parallel representing the epithelium and a resistor in series to this unit representing the subepithelium. Due to the frequency-dependent electrical characteristics of the capacitor, R^t is obtained at low

Table 1. Genotypic analysis of offspring from heterozygous × heterozygous breeding pairs

No. (%) of indicated genotypes			
Wild-type	Heterozygous	Homozygous	Total
78 (25)	170 (53)	70 (22)	318 (100)

frequencies, whereas the R^{sub} is obtained at high frequencies. The R^e was obtained from $R^e = R^t - R^{sub}$ (Gitter *et al.*, 1998).

Energy Dispersive X-ray Microanalysis (EDX)

Epon sections ~0.2 μm in thickness were examined with a 1200EX electron microscope (JEOL) equipped with EDX

Blood and Urine Profiles

Whole blood was collected directly from the heart of each mouse, and immediately centrifuged to remove blood cells from the plasma. The collected plasma was used to examine the blood profiles. The urine was collected from each mouse for 24 h in a metabolic cage. The supernatant after centrifugation was used to examine the urine profile.

RESULTS

Generation of Occludin-deficient Mice

To explore the function of occludin in vivo, we produced mice unable to express occludin. As previously reported (Saitou *et al.*, 1998), we used a mouse occludin cDNA fragment as a probe to isolate the mouse occludin gene from a λ phage 129/Sv mouse genomic library, and the identity of this gene was confirmed by nucleotide sequencing (Figure 1A). The putative exon 2 contained the first ATG, and exon 3 encoded the NH_2-terminal half of the occludin molecule from the first transmembrane domain to the second extracellular loop. Two types of targeting vectors, vector I and II, for disrupting the gene by homologous recombination in ES cells were designed and constructed (Figure 1A). These targeting vectors replace the entire exon 3 with the neomycin resistance gene or LacZ/neomysin resistance gene, respectively. Two independent lines of mice were generated from distinct ES cell clones, the occludin gene of which had been disrupted by using vector I or II. Disruption of the occludin gene in these mice was confirmed by Southern blotting analysis (Figure 1B) and PCR. RT-PCR (Figure 1C) and Western blotting with anti-occludin mAb showed that the occludin mRNA and protein, respectively, were absent in these mice. Because both lines of mice showed the same phenotype, we will mainly represent data obtained from the line generated with vector I.

No obvious phenotype was apparent in heterozygous mutant mice, and when these were interbred, wild-type, heterozygous, and homozygous mutant mice were produced in the expected Mendelian ratios (Table 1). As shown in Figure 2, at birth, the average weight of homozygotes (male = 7; female = 7) was similar to that of wild-type littermates (male = 7; female = 7). However, after birth, the average body weights of occludin −/− mice began to lag behind the wild-type and heterozygous littermates, and this difference

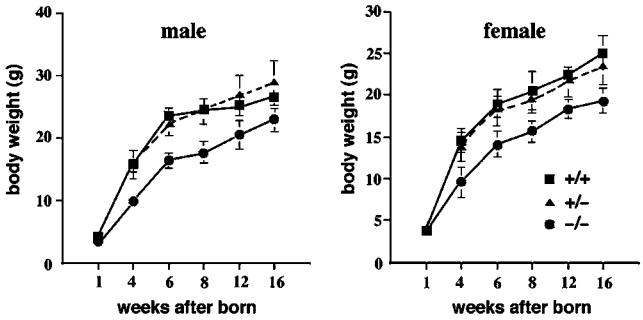

Figure 2. Postnatal growth retardation of occludin −/− mice. Occludin −/−, +/−, and +/+ mice of both sexes were born with similar body weights, but around 4 wk of age the average body weights of occludin −/− mice began to lag behind those of occludin +/− and +/+ mice (n = 7 for each). After 6 wk of age, occludin −/− mice were visibly and significantly smaller than their wild-type/heterozygous littermates.

increased further with age. Growth retardation was independent of sex; male and female homozygotes were 72 and 77% of normal weight at 8 wk of age, respectively. These findings indicated that occludin was not important for growth in utero but was required for normal postnatal growth.

No wild-type females produced any litters when mated for extended periods (~3 mo) with occludin −/− males (n = 20). In contrast, occludin −/− females (n = 20) produced litters normally when mated with wild-type males, but they did not suckle their litters, resulting in neonatal death.

Normal Morphology and Barrier Function of Tight Junctions in Intestinal Epithelial Cells

We compared components and morphology of TJs in intestinal epithelial cells between 6-wk-old wild-type and occludin −/− mice. Immunofluorescence microscopy of frozen sections revealed that both occludin and claudin-3 were exclusively concentrated at the most apical part of lateral membranes in wild-type intestinal epithelial cells (Figure 3, a and b). In occludin −/− mice, occludin was completely absent from these junctional areas, but the expression and subcellular localization of claudin-3 did not appear to be affected (Figure 3, c and d). No significant changes were detected in the expression or localization of other junctional proteins such as ZO-1, ZO-2, E-cadherin, and α-catenin (our unpublished results). Ultrathin-section electron microscopy identified the belts of typical TJs in occludin −/− mice, the size and the morphology of which could not be distinguished from those of wild-type mice (Figure 3e). When these TJs in occludin −/− mice were examined by freeze-fracture replica electron microscopy, well-developed networks of TJ strands/grooves were clearly observed (Figure 3f): There were no significant differences in the appearance or number of TJ strands/grooves between wild-type and occludin −/− mice. Similarly to the intestine, TJs did not appear to be affected in the kidney or liver in occludin −/− mice on immunofluorescence microscopy or electron microscopy (our unpublished results).

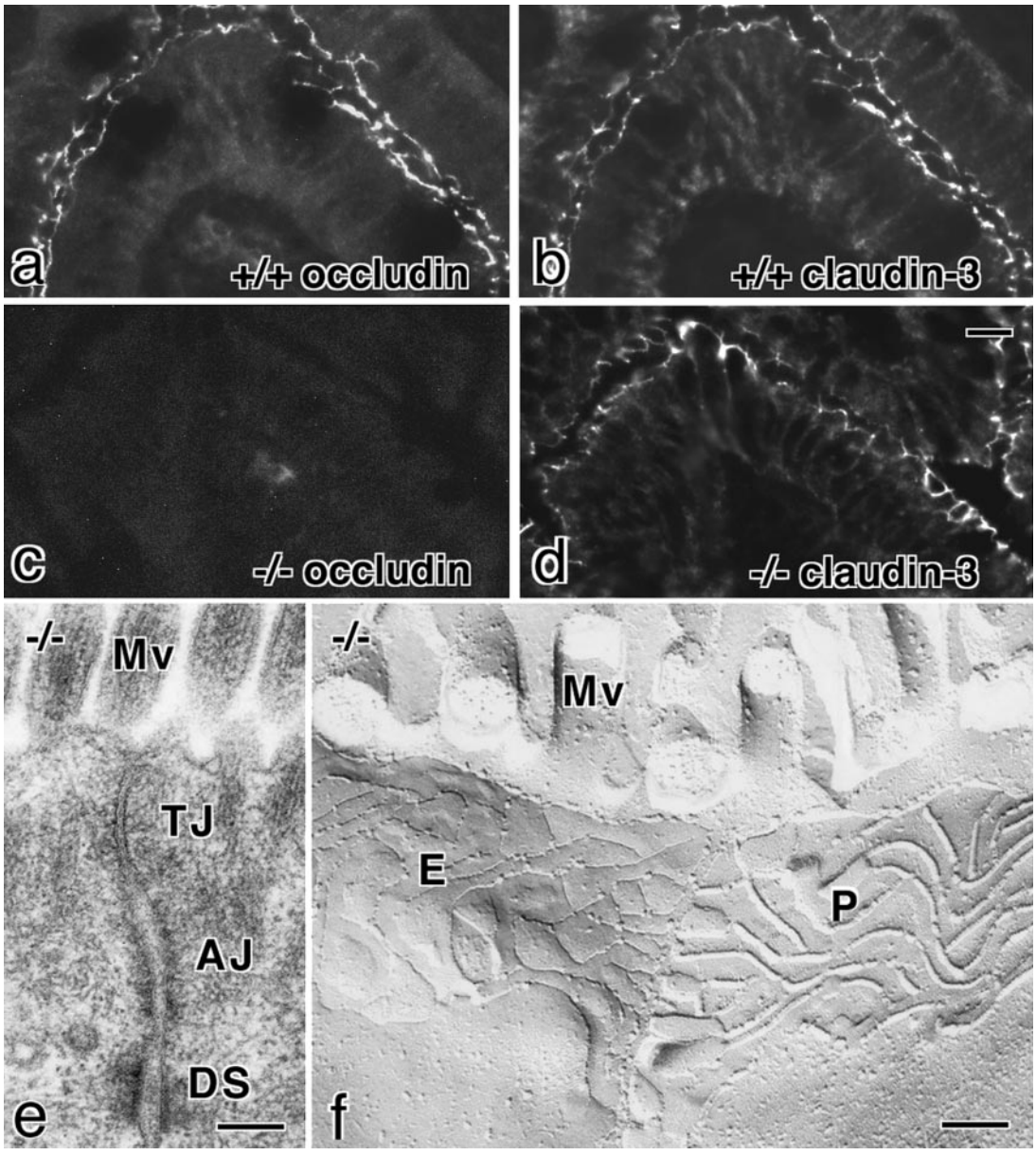

Figure 3. Tight junctions in occludin −/− mice. a–d, Immunofluorescence microscopy of frozen sections of intestinal epithelial cells of occludin +/+ (a and b) and −/− (c and d) mice with anti-occludin mAb (a and c) or anticlaudin-3 polyclonal antibody (b and d). The subcellular localization of claudin-3 did not appear to be affected by the loss of occludin expression. (e and f) Ultrathin-section (e) and freeze-fracture replica (f) images of the junctional complex region of intestinal epithelial cells of occludin −/− mice. TJs and tight junction strands/grooves were indistinguishable from those in occludin +/+ mice. AJ, adherens junction; DS, desmosome; Mv, microvilli; P, P-face; E, E-face. Bars, 10 μm for a–d and 0.1 μm for e and f.

Next, we performed an impedance analysis to measure the epithelial and subepithelial resistance of the small and large intestine of wild-type as well as occludin −/− mice (Table 2). In this analysis, R^e represents the resistance of the epithelial layer itself, and R^{sub} represents the resistance of the underlying connective tissues and muscles, which is elevated in inflammation. This technique has been shown to detect even small changes in R^e from mice, rat, and human and is thus superior to the conventional Ussing technique to evaluate the epithelial barrier function of intestinal epithelia (Gitter *et al.*, 1998, 2000). As shown in Table 2, both in occludin +/− and −/− mice, compared with the wild-type mice, no significant difference was detected in R^e as well as R^{sub} of the small and large intestine. We then concluded that the barrier function of TJs in the intestinal epithelium of occludin −/− mice is normal at least in terms of the transepithelial resistance.

Table 2. Epithelial barrier function of the small and large intestine of occludin +/+ and −/− mice

	Small intestine		Large intestine	
	R^e	R^{sub} ($\Omega \cdot cm^2$)	R^e	R^{sub} ($\Omega \cdot cm^2$)
Wild-type	22 ± 6 (6)	33 ± 6 (6)	70 ± 5 (7)	18 ± 2 (7)
Occludin +/−	23 ± 3 (8)^{NS}	44 ± 4 (8)^{NS}	70 ± 7 (8)^{NS}	14 ± 1 (8)^{NS}
Occludin −/−	18 ± 2 (10)^{NS}	34 ± 3 (10)^{NS}	65 ± 5 (10)^{NS}	21 ± 4 (10)^{NS}

NS, no significant difference versus control.

R^e and R^{sub} were measured by alternating current impedance analysis from 16-wk-old mice. Results are means ± SEM (n, number of mice analyzed).

Chronic Gastritis and Successive Hyperplasia in the Gastric Epithelium

Histological examination revealed marked changes in the gastric mucosa of occludin −/− mice. These changes were detected only in gastric gland regions but not in pyloric gland regions. At 3–6 wk of age, occludin −/− mice showed marked loss of normal differentiation of the epithelium in gastric glands (Figure 4, a and b). The most striking findings were the consistent loss of gastric chief cells, severe decrease in number of parietal cells, and the occurrence of abnormal mucoid-containing cells. Occludin −/− mice began to develop gastritis around 10 wk of age, which became very severe around 28 wk of age. Abnormal glands with multiple branches were present (Figure 4d), and severe inflammatory infiltrates were seen in the glands (Figure 4e). The infiltrate involved the mucosa and lamina propria and extended to the tops of the glandular mucosa. At 40 wk of age, the mucosa of occludin −/− mice was seen to be thickened on gross inspection. Compared with wild-type mice (Figure 4f), the gastric mucosa was obviously thickened, although the infiltration was less severe at this stage (Figure 4, g–i). In most portions of the stomach fundus, gastric glands were lined with epithelium exhibiting cellular crowding, nuclear pleomorphism, increased nuclear:cytoplasmic ratio, and loss of nuclear polarity (Figure 4, g and h), but in some portions gastric glands appeared to be transformed into a pyloric gland-like appearance characterized by the presence of numerous mucoid-containing cells (Figure 4i).

Calcification in the Brain

A striking neuropathological finding in occludin −/− mice was the progressive accumulation of mineral deposits in the cerebellum and basal ganglia (Figure 5). Small and scattered deposits were observed as early as 9 wk after birth, and their size and number increased progressively with age, resulting in concentric, often laminated deposits. Electron microscopy with EDX microanalysis indicated that these inclusions were composed almost entirely of calcium and coprecipitating phosphorus (Figure 5e). Small granular calcium deposits were often localized along small vessels, mainly venules and capillaries (Figure 5d).

Abnormalities in the Testis, Salivary Gland, and Bone

In the testis of occludin −/− mice at 6 wk of age, the seminiferous tubules were normally developed with normal germ cells (Figure 6, a and b). However, when mice became older around 40 to 60 wk of age, tubules showed typical atrophy (Figure 6, c and d). The atrophied tubules were devoid of germ cells and retained only Sertoli cells along the basement membrane (Figure 6, e and f). When the salivary glands of occludin −/− mice were compared with those of wild-type controls, there appeared to be no difference in acinar cells, but a marked difference was found in the appearance of striated ducts. In occludin −/− mice, striated duct cells lacked characteristic cytoplasmic granules (Figure 6, g and h). Finally, abnormalities were also found in the bone. Figure 7 shows transverse sectional views of the femur bone from 40- and 60-wk-old male mice by x-ray computer tomograpy. In occludin −/− mice, the compact bone was significantly thinner than that of wild-type controls (n = 4).

Serum and Urine

Because the mineral deposition in the brain as well as the bone atrophy suggested the abnormalities for Ca^{2+} ion metabolism in occludin −/− mice, we compared blood and urine profiles between occludin −/− and wild-type mice with special attention to Ca^{2+} and PO_4^{2-}. However, occludin −/− mice were not distinguishable from wild-type mice with respect to these profiles (Tables 3 and 4).

DISCUSSION

We previously reported that occludin −/− ES cells can be differentiated into visceral endoderm cells that bear well-developed network of TJ strands (Saitou *et al*., 1998), and that claudins can reconstitute TJ strands in L fibroblasts without occludin (Furuse *et al*., 1998a,b). Furthermore, as shown in this study, in occludin −/− mice, the tissues such as the intestine, liver, and kidney bore TJs that were morphologically indistinguishable from those of wild-type controls. These findings clearly indicated that occludin is not required for the formation of TJ strands per se. On the other hand, previous studies suggested the direct involvement of occludin in the barrier function of TJs (Balda *et al*., 1996; Chen *et al*., 1997; Wong and Gumbiner, 1997). However, TJ strands in occludin-deficient visceral endoderm functioned

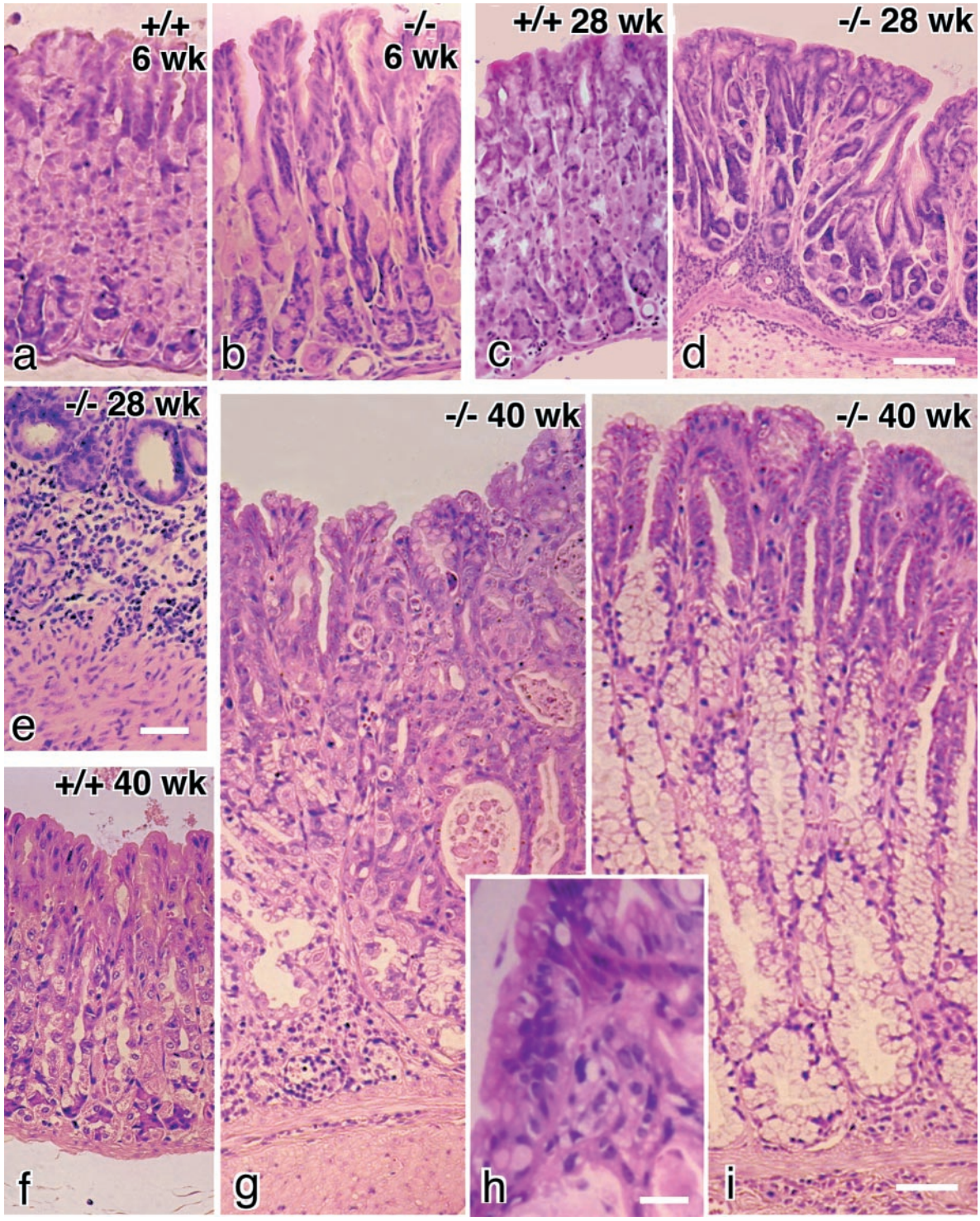

Figure 4. Chronic inflammation and successive hyperplasia in gastric epithelium in occludin −/− mice. Paraffin sections were stained with hematoxylin-eosin. At 6 wk of age, compared with wild-type mice (a), the gastric epithelium of occludin −/− mice was characterized by the loss of chief cells, a decrease in number of parietal cells, and the occurrence of abnormal mucoid-containing cells (b). Around 28 wk of age (c, wild-type), severe inflammatory infiltrates (e) were seen in the abnormal gastric glands with multiple branches in occludin −/− mice (d). In older occludin −/− mice around 40 wk of age, compared with wild-type mice (f) the gastric mucosa was significantly thickened (g and i). In some cases, the thickened gastric epithelium was characterized by cellular crowding, nuclear pleomorphism, increased nuclear:cytoplasmic ratio, and loss of nuclear polarity (g and h), and in other cases, the gastric glands had a pyloric gland-like appearance (i). Bars, 100 μm for a–d, f, g, and i; 40 μm for e; and 10 μm for h.

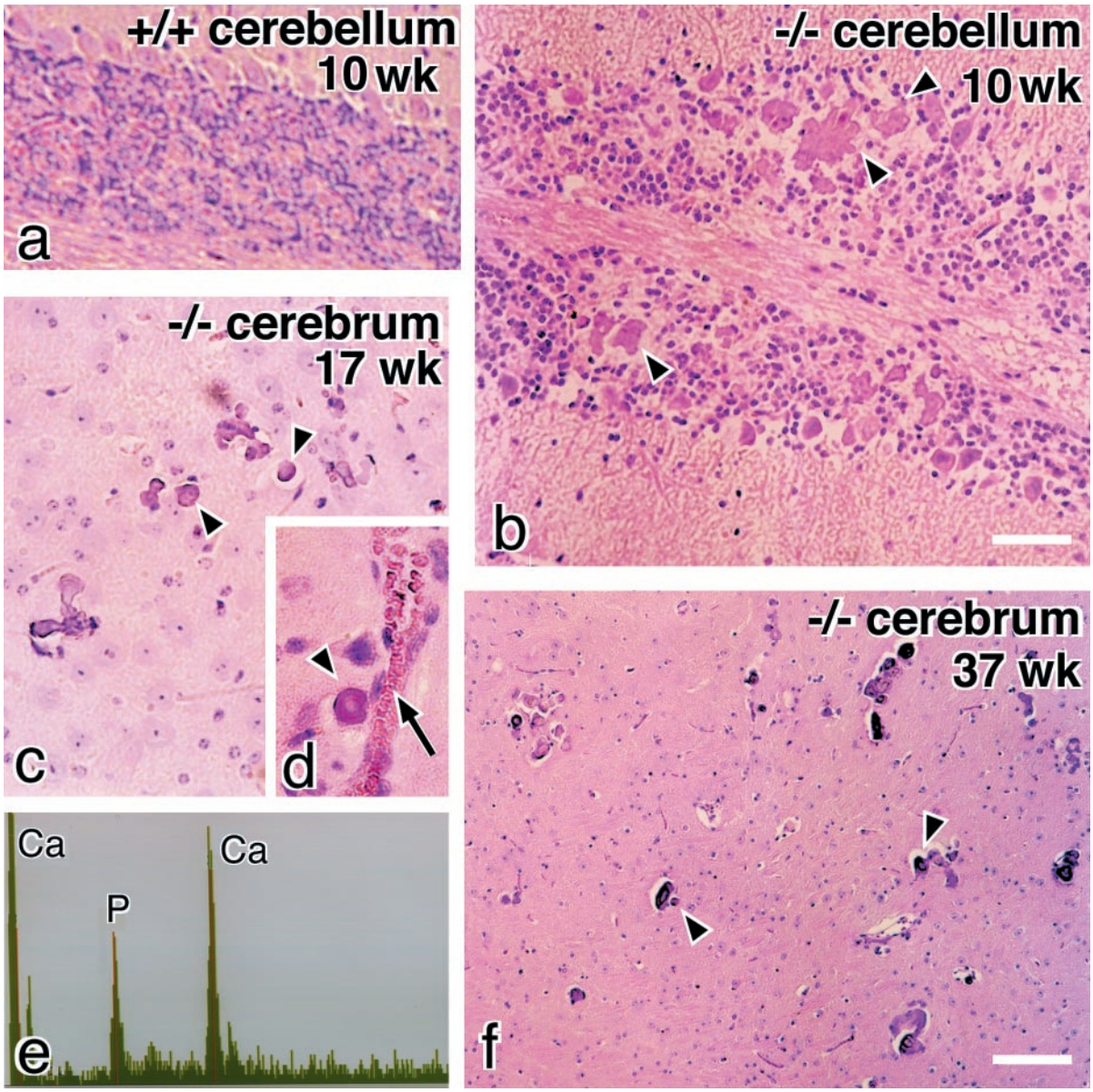

Figure 5. Calcification in the brain of occludin −/− mice. Paraffin sections of the cerebellum (a and b) and basal ganglia (c, d, and f) were stained with hematoxylin-eosin. Numerous concentric, often laminated mineral deposits (arrowheads) were observed in the cerebellum (b) and basal ganglia (c, d, and f) in occludin −/− mice. These deposits were often localized along small vessels (arrow in d). This kind of deposit was not found in the brain of wild-type mice (a). EDX analysis of these deposits showed calcium and phosphorus peaks similar to those of hydroxyapatite (e). Bars, 100 μm for a and b, and 200 μm for c, d, and f.

as barriers at least in vitro (Saitou *et al*., 1998), and in this study we detected no dysfunction of the TJ barrier electrophysiologically in intestinal epithelial cells of occludin −/− mice (Table 2).

The question has naturally arisen as to what is the physiological function of occludin in vivo. Although occludin −/− mice were born in the expected Mendelian ratios, occludin −/− mice showed very complex gross and histological phenotypes as described in this study. The most characteristic gross phenotype of occludin −/− mice was their postnatal growth retardation. Furthermore, no histological abnormality was found in the testis as well as the ovary at least during their reproductive period, but their sexual behavior appeared to be affected: Occludin −/− males with normal spermatogenesis produced no litters when mated with wild-type females, and occludin −/− females produced litters normally when mated with wild-type males but did not suckle them. Histological abnormalities were found in several tissues in occludin −/− mice; chronic inflammation and hyperplasia of the gastric epithe-

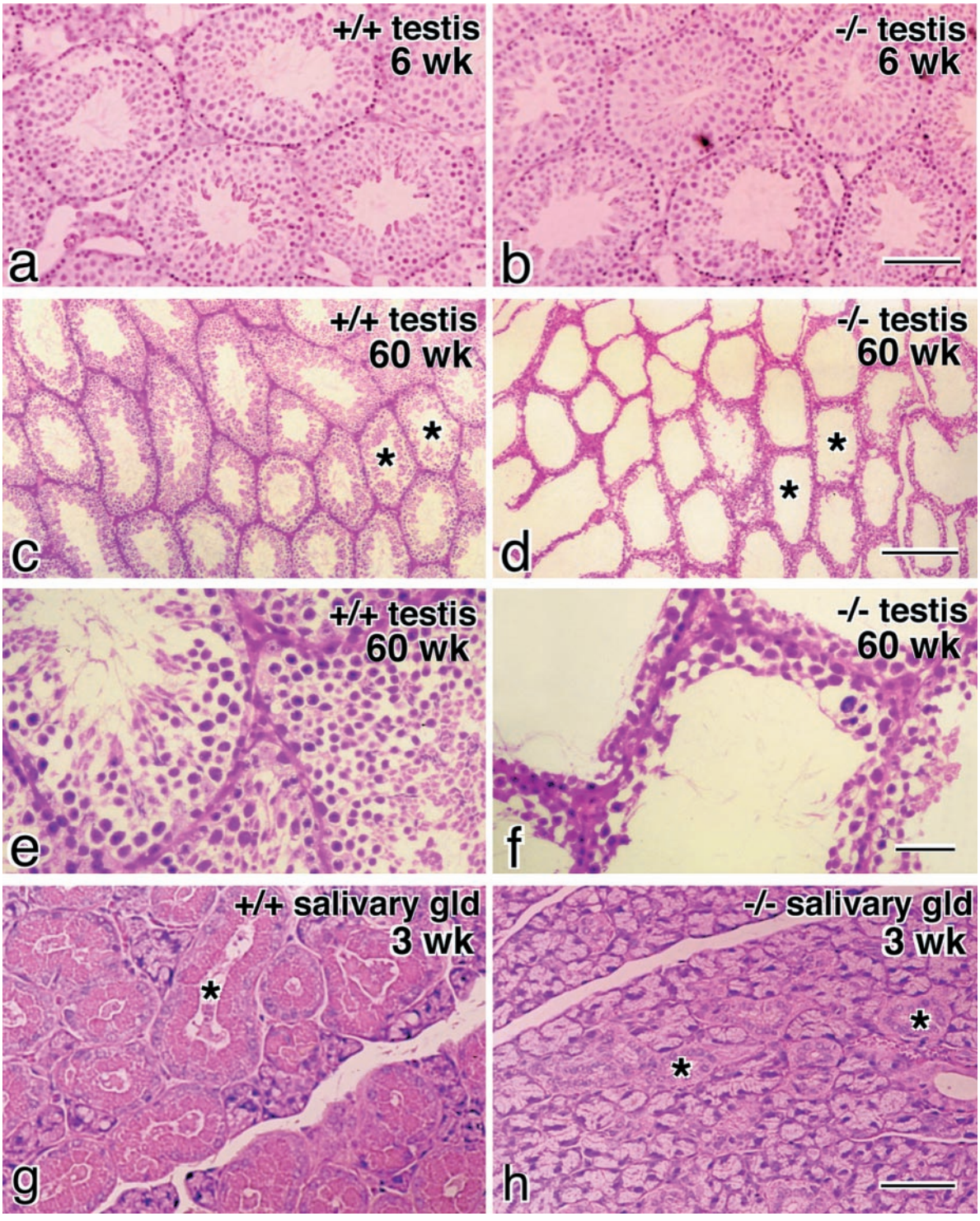

Figure 6. Testis and salivary gland in occludin −/− mice. Paraffin sections of the testis from 6-wk-old (a and b) or 60-wk-old mice (c–f) and the salivary gland from 3-wk-old mice (g and h) were stained with hematoxylin-eosin. In young occludin −/− mice, the testis was normally developed with normal germ cells (a and b), but in older mice the seminiferous tubules showed typical atrophy (d and f) compared with those in wild-type mice (c and e). The atrophied tubules were devoid of germ cells and retained only Sertoli cells (f). When the salivary gland of occludin −/− mice (h) was compared with that of wild-type mice (g), it was clear that striated duct cells (asterisks) in occludin −/− mice lacked cytoplasmic granules. Bars, 100 μm for a and b, 200 μm for c and d, 40 μm for e and f, and 100 μm for g and h.

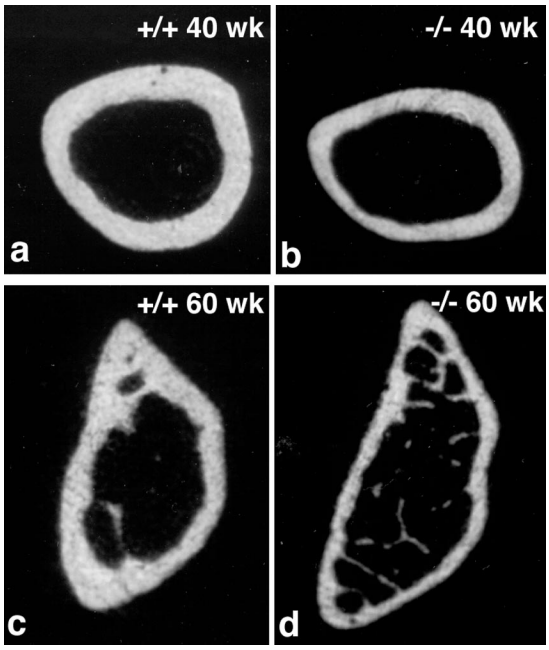

Figure 7. X-ray computer tomography of the femur bone. Compared with wild-type mice (a and c), the compact bone was significantly thinner in occludin −/− mice (b and d).

lium, calcification in the brain, testicular atrophy (only in old mice), loss of cytoplasmic granules in striated duct cells of the salivary gland, and thinning of the compact bone. However, no abnormalities were detected in blood or urine profiles, and it was very difficult to relate the above-mentioned complex phenotypes in occludin −/− mice with each other.

It was also difficult to explain any of these phenotypes of occludin −/− mice from the viewpoint of the functions of TJs. One possible explanation is as follows: Although the impedance analysis did not detect significant differences in epithelial resistance of the small and large intestine between wild-type and occludin −/− mice, the lack of occludin in TJ strands may change some aspect of the barrier function of TJs, and this barrier dysfunction would induce gastritis and/or affect the absorption of Ca^{2+} through the paracellular pathway of the gastrointestinal epithelium, leading to calcification in the brain/thinning of the compact bone. Inconsistent with this explanation, however, the serum levels of Ca^{2+} and PO_4^{2-} (Table 3) as well as parathyroid hormone (our unpublished results) were normal in occludin −/− mice. Furthermore, because the barrier functions of TJs in Sertoli cells are believed to be important for the spermatogenesis, the testicular atrophy observed in old occludin −/− mice would also be explained by some change in the TJ barrier due to the absence of occludin from TJ strands. However, again in consistent with this explanation, occludin was expressed in mouse Sertoli cells, but not in human Sertoli cells, indicating that in human the spermatogenesis proceeds normally without the expression of occludin in Sertoli cells (Moroi *et al*., 1998).

Alternatively, in wild-type mice, occludin, especially its cytoplasmic domain, may be involved in some intracellular signaling, and the lack of occludin may affect the differentiation of gastric epithelial cells and salivary gland cells. The cytoplasmic domain of occludin is heavily phosphorylated in TJ strands (Sakakibara *et al*., 1997), and various signaling molecules have been reported to associate with the cytoplasmic surface of TJ strands (Tsukita *et al*., 1999). Furthermore, the forced expression of occludin was recently shown to suppress the v-raf-induced transformation of cultured epithelial cells (Li and Mrsny, 2000). These findings suggested the possible involvement of occludin in some intracellular signaling. Because the molecular mechanism behind occludin-based signaling is fragmentary at the cellular level, it is still premature to further discuss the phenotypes of occludin −/− mice from the viewpoint of intracellular signaling, but any discussion must explain why the differentiation of gastric epithelial cells and salivary duct cells, but not other types of cells such as intestinal epithelial cells, were affected in occludin −/− mice.

Two types of occludin were shown to be generated from a single gene by alternative splicing (Muresan *et al*., 2000), but judging form their structures our occludin −/− mice were expected to lack both occludin variants. To date, despite intensive efforts, no occludin-like genes have yet been identified (Tsukita and Furuse, 1999). Therefore, it is not likely that the functional redundancy of occludin-like genes can explain the complex phenotypes of occludin −/− mice.

Of course, it is also possible that the complex phenotype of occludin −/− mice is attributed to an as yet unidentified function of TJs. What we can conclude at present is that the occludin gene is indispensable in each species. Further detailed analyses of the functions of occludin at the cellular level are required for better understanding of the molecular mechanism behind the complex phenotypes of occludin −/− mice.

ACKNOWLEDGMENTS

We thank Dr. S. I. Nishikawa (Kyoto University) for help with histological analyses of mouse tissues. We also thank all the members of our laboratory (Department of Cell Biology, Faculty of

Table 3. Blood profiles for occludin +/+ and −/− mice

		Ca^{2+} (mg/dl)	PO_4^{-} (mg/dl)	Albumin (mg/dl)
+/+	Female	8.8 ± 0.3 (10)	7.2 ± 0.8 (10)	2.8 ± 0.3 (10)
	Male	9.2 ± 0.6 (7)	6.8 ± 1.0 (7)	2.8 ± 0.3 (7)
−/−	Female	8.7 ± 0.3 (11)	6.9 ± 1.0 (11)	2.8 ± 0.4 (11)
	Male	8.7 ± 0.3 (9)	6.4 ± 0.6 (9)	2.7 ± 0.3 (9)

Results are means ± SD (n, number of mice analyzed). Assays were performed using serum collected from 15- to 30-wk-old mice.

Table 4. Urine profiles for occludin +/+ and −/− mice

	Na^+ (mEq/g h)	K^+ (mEq/g h)	Ca^{2+} (mg/g h)	Mg^{2+} (mg/g h)	Cl^- (mEq/g h)	PO_4^{2-} (mg/g h)	BUN (mg/g h)	Creatinin (mg/g h)
+/+	271 ± 132	617 ± 209	1.8 ± 0.8	11 ± 5	517 ± 210	33 ± 11	768 ± 346	9.4 ± 3.4
−/−	260 ± 154	629 ± 236	1.5 ± 0.9	12 ± 8	585 ± 224	39 ± 14	833 ± 211	10.8 ± 2.2

Results are means ± SD. Assays were performed using urine collected from 15- to 30-wk-old male mice (n = 6). The data shown are representative of two independent experiments that gave similar results. BUN, blood urea nitrogen.

Medicine, Kyoto University) for helpful discussions. This study was supported in part by a grant-in-aid for Cancer Research and a grant-in-aid for Scientific Research (A) from the Ministry of Education, Science, and Culture of Japan.

REFERENCES

Anderson, J.M., and van Itallie, C.M. (1995). Tight junctions and the molecular basis for regulation of paracellular permeability. Am. J. Physiol. *269*, G467–G475.

Ando-Akatsuka, Y., Saitou, M., Hirase, T., Kishi, M., Sakakibara, A., Itoh, M., Yonemura, S., Furuse, M., and Tsukita, Sh. (1996). Interspecies diversity of the occludin sequence: cDNA cloning of human, mouse, dog, and rat-kangaroo homologues. J. Cell Biol. *133*, 43–47.

Balda, M.S., Whitney, J.A., Flores, C., González, S., Cereijido, M., and Matter, K. (1996). Functional dissociation of paracellular permeability and transepithelial electrical resistance and disruption of the apical-basolateral intramembrane diffusion barrier by expression of a mutant tight junction membrane protein. J. Cell Biol. *134*, 1031–1049.

Chen, Y.-H., Merzdorf, C., Paul, D.L., and Goodenough, D.A. (1997). COOH terminus of occludin is required for tight junction barrier function in early *Xenopus* embryos. J. Cell Biol. *138*, 891–899.

Chomczynski, P., and Sacchi, N. (1987). Single-step method of RNA isolation by acid guanidinium thiocyanate-phenol-chloroform extraction. Anal. Biochem. *162*, 156–159.

Farquhar, M.G., and Palade, G.E. (1963). Junctional complexes in various epithelia. J. Cell Biol. *17*, 375–412.

Furuse, M., Fujita, K., Hiiragi, T., Fujimoto, K., and Tsukita, Sh. (1998a). Claudin-1 and -2: novel integral membrane proteins localizing at tight junctions with no sequence similarity to occludin. J. Cell Biol. *141*, 1539–1550.

Furuse, M., Hirase, T., Itoh, M., Nagafuchi, A., Yonemura, S., Tsukita, Sa., and Tsukita, Sh. (1993). Occludin: a novel integral membrane protein localizing at tight junctions. J. Cell Biol. *123*, 1777–1788.

Furuse, M., Sasaki, H., Fujimoto, K., and Tsukita, Sh. (1998b). A single gene product, claudin-1 or -2, reconstitutes tight junction strands and recruits occludin in fibroblasts. J. Cell Biol. *143*, 391–401.

Gitter, A.H., Bendfeldt, K., Schulzke, J.D., and Fromm, M. (2000). Trans-/paracellular, surface/crypt, and epithelial/subepithelial resistances of mammalian colonic epithelia. Pflügers Arch. *439*, 477–482.

Gitter, A.H., Fromm, M., and Schulzke, J.D. (1998). Impedance analysis for determination of epithelial and subepithelial resistance in intestinal tissues. J. Biochem. Biophys. Methods *37*, 35–46.

Goodenough, D.A. (1999). Plugging the leaks. Proc. Natl. Acad. Sci. USA *96*, 319–321.

Gumbiner, B. (1987). Structure, biochemistry, and assembly of epithelial tight junction. Am. J. Physiol. *253*, C749–C758.

Gumbiner, B. (1993). Breaking through the tight junction barrier. J. Cell Biol. *123*, 1631–1633.

Hirase, T., Staddon, J.M., Saitou, M., Ando-Akatsuka, Y., Itoh, M., Furuse, M., Fujimoto, K., Tsukita, Sh., and Rubin, L.L. (1997). Occludin as a possible determinant of tight junction permeability in endothelial cells. J. Cell Sci. *110*, 1603–1613.

Keller, G., Kennedy, M., Papayannopoulou, T., and Wiles, M.V. (1993). Hematopoietic commitment during embryonic stem cell differentiation in culture. Mol. Cell. Biol. *13*, 473–486.

Li, D., and Mrsny, R.J. (2000). Oncogenic Raf-1 disrupts epithelial tight junctions via downregulation of occludin. J. Cell Biol. *148*, 791–800.

McCarthy, K.M., Skare, I.B., Stankewich, M.C., Furuse, M., Tsukita, Sh., Rogers, R.A., Lynch, R.D., and Schneeberger, E.E. (1996). Occludin is a functional component of the tight junction. J. Cell Sci. *109*, 2287–2298.

Morita, K., Furuse, M., Fujimoto, K., and Tsukita, Sh. (1999a). Claudin multigene family encoding four-transmembrane domain protein components of tight junction strands. Proc. Natl. Acad. Sci. USA *96*, 511–516.

Morita, K., Sasaki, H., Fujimoto, K., Furuse, M., and Tsukita, Sh. (1999b). Claudin-11/OSP-based tight junctions in myelinated sheaths of oligodendrocytes and Sertoli cells in testis. J. Cell Biol. *145*, 579–588.

Morita, K., Sasaki, H., Furuse, M., and Tsukita, Sh. (1999c). Endothelial claudin: claudin-5/TMVCF constitutes tight junction strands in endothelial cells. J. Cell Biol. *147*, 185–194.

Moroi, S., Saitou, M., Fujimoto, K., Sakakibara, A., Furuse, M., Yoshida, O., and Tsukita, Sh. (1998). Occludin is concentrated at tight junctions of mouse/rat but not human/guinea pig Sertoli cells in testes. Am. J. Physiol. *274*, C1708–C1717.

Muresan, Z., Paul, D.L., and Goodenough, D.A. (2000). Occludin 1B, a variant of the tight junction protein occludin. Mol. Biol. Cell *11*, 627–634.

Rodriguez-Boulan, E., and Nelson, W.J. (1989). Morphogenesis of the polarized epithelial cell phenotype. Science *245*, 718–725.

Saitou, M., Ando-Akatsuka, Y., Itoh, M., Furuse, M., Inazawa, J., Fujimoto, K., and Tsukita, Sh. (1997). Mammalian occludin in epithelial cells: its expression and subcellular distribution. Eur. J. Cell Biol. *73*, 222–231.

Saitou, M., Fujimoto, K., Doi, Y., Itoh, M., Fujimoto, T., Furuse, M., Takano, H., Noda, T., and Tsukita, Sh. (1998). Occludin-deficient embryonic stem cells can differentiate into polarized epithelial cells bearing tight junctions. J. Cell Biol. *141*, 397–408.

Sakakibara, A., Furuse, M., Saitou, M., Ando-Akatsuka, Y., and Tsukita, Sh. (1997). Possible involvement of phosphorylation of occludin in tight junction formation. J. Cell Biol. *137*, 1393–1401.

Schneeberger, E.E., and Lynch, R.D. (1992). Structure, function, and regulation of cellular tight junctions. Am. J. Physiol. *262*, L647–L661.

Staehelin, L.A. (1973). Further observations on the fine structure of freeze-cleaved tight junctions. J. Cell Sci. *13*, 763–786.

Staehelin, L.A. (1974). Structure and function of intercellular junctions. Int. Rev. Cytol. *39*, 191–283.

Tsukita, Sh., and Furuse, M. (1999). Occludin and claudins in tight junction strands: leading or supporting players? Trends Cell Biol. *9*, 268–273.

Tsukita, Sh., and Furuse, M. (2000). Pores in the wall: claudins constitute tight junctions strands containing aqueous pores. J. Cell Biol. *149*, 13–16.

Tsukita, Sh., Itoh, M., and Furuse, M. (1999). Structural and signaling molecules come together at tight junctions. Curr. Opin. Cell Biol. *11*, 628–633.

Wong, V., and Gumbiner, B.M. (1997). A synthetic peptide corresponding to the extracellular domain of occludin perturbs the tight junction permeability barrier. J. Cell Biol. *136*, 399–409.